Shifting hail hazard under global warming

Timothy H. Raupach[1,2,3*], Raphael Portmann[4,5], Christian Siderius[6], Steven C. Sherwood[2,3]

[1]Institute for Climate Risk and Response, UNSW Sydney, Mathews Building Level 4, The University of New South Wales, Sydney, 2051, NSW, Australia.
[2]Climate Change Research Centre, UNSW Sydney, Australia.
[3]ARC Centre of Excellence for Climate Extremes, UNSW Sydney, Australia.
[4]Agroscope, Swiss Federal Office for Agriculture, Zurich, Switzerland.
[5]Planval, Bern, Switzerland.
[6]Uncharted Waters Research, Sydney, Australia.

*Corresponding author(s). E-mail(s): timothy.h.raupach@gmail.com;

Abstract

Hailstorms cause significant damage across the globe, but changes to hailstorms in a warming climate are not well quantified. Here, we applied hail proxies to global model projections to quantify changes in the frequency of hail-prone conditions and the effects of those changes on 26 crop types. In projections with 2 °C and 3 °C of mean global warming, hail-prone conditions shift poleward, causing decreases in hail frequency across the mid-latitudes and increases in colder regions. In general, hail-prone frequency decreases in summer and increases in winter, leading to projected increases in the hail-prone proportion of cropping season for winter crops and decreases for summer crops.

Keywords: hail, severe weather, convection, trends, projections

Hailstorms are a form of extreme weather that causes significant damage to physical assets including crops. Hail and the storms that produce it are expected to be affected by anthropogenic global warming, yet regional studies using observations or projections show geographical inhomogeneities and there remains high uncertainty on the details of any changes [1–3]. Globally, hail observations are scarce [3], meaning global climatologies generally rely on satellite data [4, 5] or examination of environmental conditions in reanalyses using hail proxies [6]. Here, we produced global projections of future hail hazard using hail proxies applied to model output from the Coupled Model Intercomparison Project (CMIP6) [7] in a per-degree framework.

Because hailstorms are hard to observe and model given their small spatial size and relative rarity [3], proxies that detect hail-prone atmospheric conditions are often used in climatological studies. Hail proxies rely on detecting the atmospheric "ingredients" required for hail to form. Hailstones form by accretion of supercooled liquid water onto ice embryos suspended in the updraft of a thunderstorm, until they become too heavy to support, and fall while undergoing melt on their descent through warmer air [8, 9]. Hailstorm ingredients are usually considered to include, at a minimum, atmospheric instability, for a thunderstorm with strong updrafts that can support hail growth to form [10], and vertical wind shear (horizontal wind differences by height) to "organise" the storm [11] and influence hailstone trajectories [12, 13]. Instability–shear hail proxies are common [14]. Proxies suffer from the "initiation problem" because storms rarely initiate even in storm-prone conditions [14–16].

Climate change is expected to affect the ingredients for hailstorms and thus the frequency and severity of hailstorms themselves [3]. A thermodynamic expectation is of three offsetting effects: first, increased instability owing to a larger saturation deficit in a warmer atmosphere [17] leading to more storm initiation and stronger updrafts that could support larger hailstones; second, increased melting of hailstones owing to a warmer troposphere [18], thus leading to a reduction (or elimination [19]) of surface hail frequency; and third, an overall decrease in vertical wind shear [11] that is generally outweighed by changes in instability **(refs)** or may not apply locally [20, 21]. The broad thermodynamic expectation is thus of a reduction in surface hail frequency combined with an increase in severity when hail does reach the Earth's surface [3]. However, regional studies show large geographical heterogeneity in signals for hail frequency, owing in part to offsetting in these climate change effects and in part to dynamical changes meaning that ingredient changes are not spatially uniform, while hail severity is generally expected to increase [3].

Here, we applied four hail proxies to an ensemble of eight global projections from CMIP6, to examine future projections of the frequency of hail-prone conditions globally. We investigated the effects of projected changes on hail-prone proportions of crop growing seasons for 26 different crops. We used a per-degree framework [22] for simpler comparisons between models. For details of the simulations and proxies used, refer to "Online methods" and the supplementary information. Our work shows how hailstorm frequency is projected to decrease in warm environments but increase in cooler environments in future, driven primarily by changes in convective instability. The changes are projected to increase the risk of hail occurrence for winter crops while decreasing occurrence risk in summer. **(Include local changes.)**

Results

Comparison to ERA5 for historical period

Figure 1 shows a comparison between the multimodel, multi-proxy mean of annual hail-prone days for the CMIP6 models, and the multi-proxy mean of annual hail-prone days for the ERA5 reanalyses. While the results for individual CMIP6 models show a wide spread of absolute values (Supplementary Figure 2), the locations of hail hotspots match well between reanalysis and models. The models MPI-ESM1-2-HR and EC-Earth show similar numbers of hail-prone days to ERA5, while MIROC6, CMCC-CM2-SR5, and CMCC-ESM2 show moderately more and CNRM-CM6-1 and GISS-E2-1-G show significantly more hail-prone days than ERA5. There are also differences across the selected hail proxies, with the Significant Hail Parameter (SHIP) [23] producing the fewest hail-prone days and the proxy of Raupach et al. 2023 without extra conditions [14] producing the greatest number of hail-prone days. Given there is geographical agreement but differences in absolute numbers of hail-prone days, we consider relative changes per model in the rest of our analyses.

Case study of hail-prone day anomalies

Monthly anomalies, derived using ERA5 reanalysis data, in proxy-derived hail-prone days show higher values for months with known high occurrences of damaging hailstorms. The proxy produced higher than average numbers of hail-prone days for February 2015 in northern and central India (Supplementary Figure 3), regions that were affected by hailstorms that caused major losses to wheat crops at this time [24]. Similarly, the proxy highlights areas of central and southern Europe as particularly hail-prone in June 2022 (Supplementary Figure 4), when the passage of two low-pressure systems caused hailstorm outbreaks across these regions [25] that broke records for insured losses in France [26]. The proxy also identified April 2015 and October 2022 as unusually hail-prone months in northeast India and western France, respectively; there were reported hailstorms in both regions during the respective months [25, 27]. These case-study results increase our confidence in the ability of the hail proxies, which were trained using data from Australia [14], Italy [28], and the United States [23] to identify hail-prone conditions worldwide.

Changes in hail-prone days with warming

Figure 2 shows multimodel, multi-proxy mean changes in annual hail-prone days for 2 °C and 3 °C of global warming, respectively. Multimodel, multi-proxy mean changes are shown as relative differences zoomed to selected land areas in Figures 3 and 4. There is an overall poleward shift of hail-prone conditions.

- **(Incorporate supplementary figures.)** Differences per model and proxy are shown in Supplementary Figures 5 and 6. Multimodel, multi-proxy mean differences by season are shown in Supplementary Figure 7.
- **(Comment on regional changes in Figures 3 and 4.)**

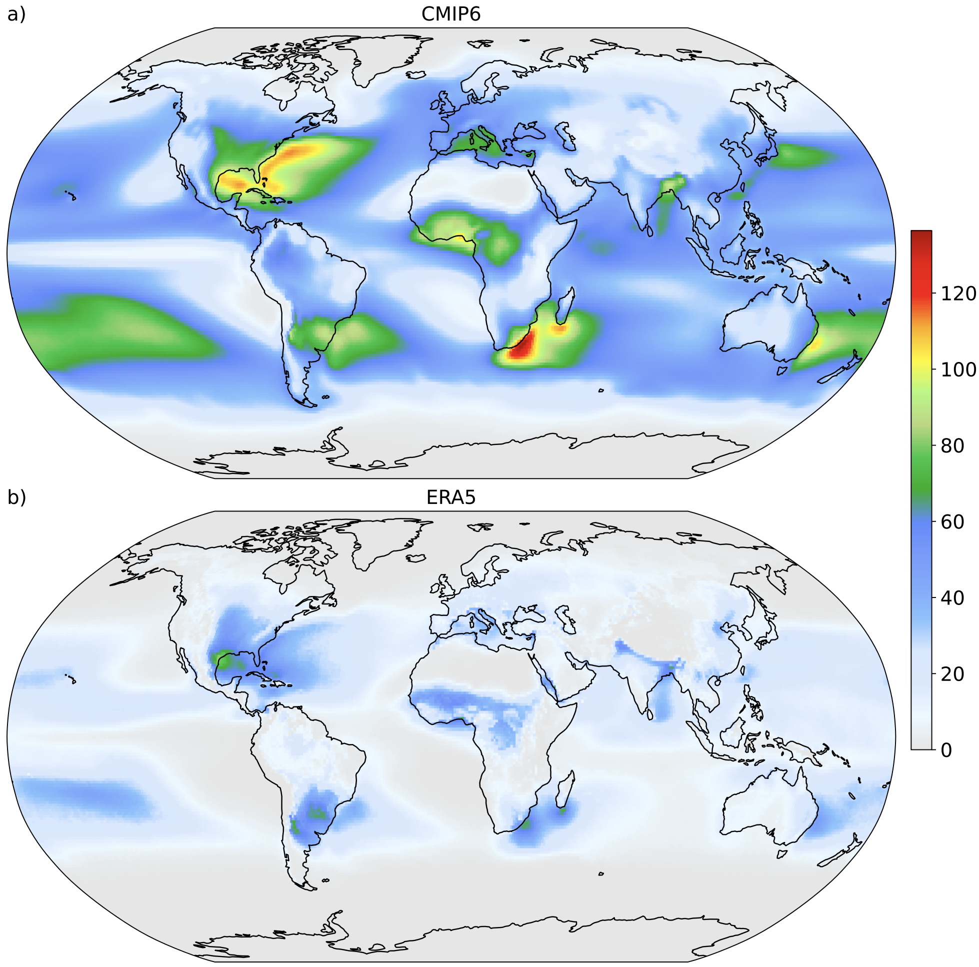

Fig. 1 Hail proxies show known hail-prone regions in both projections and reanalysis. Multimodel, multi-proxy mean annual hail-prone days for CMIP6 models (a), and multi-proxy mean annual hail-prone days for ERA5 reanalysis (b), for four selected proxies over the historical period (1980-1999) at 1×1 $^\circ$ resolution.

Drivers of the projected changes

Future projections show almost uniform increases in convective instability, with increases in extreme values of convective available potential energy (CAPE) and lifted index (LI), and increasing convective inhibition that may lead to more explosive development of severe storms (Supplementary Figure 8). Projections in extremes in 0-6 km bulk wind shear (S06) show decreases (mixed increases) in the northern (southern) hemisphere (Supplementary Figure 8). Temperature-related ingredients naturally increase in the warmer scenarios (Supplementary Figure 9).

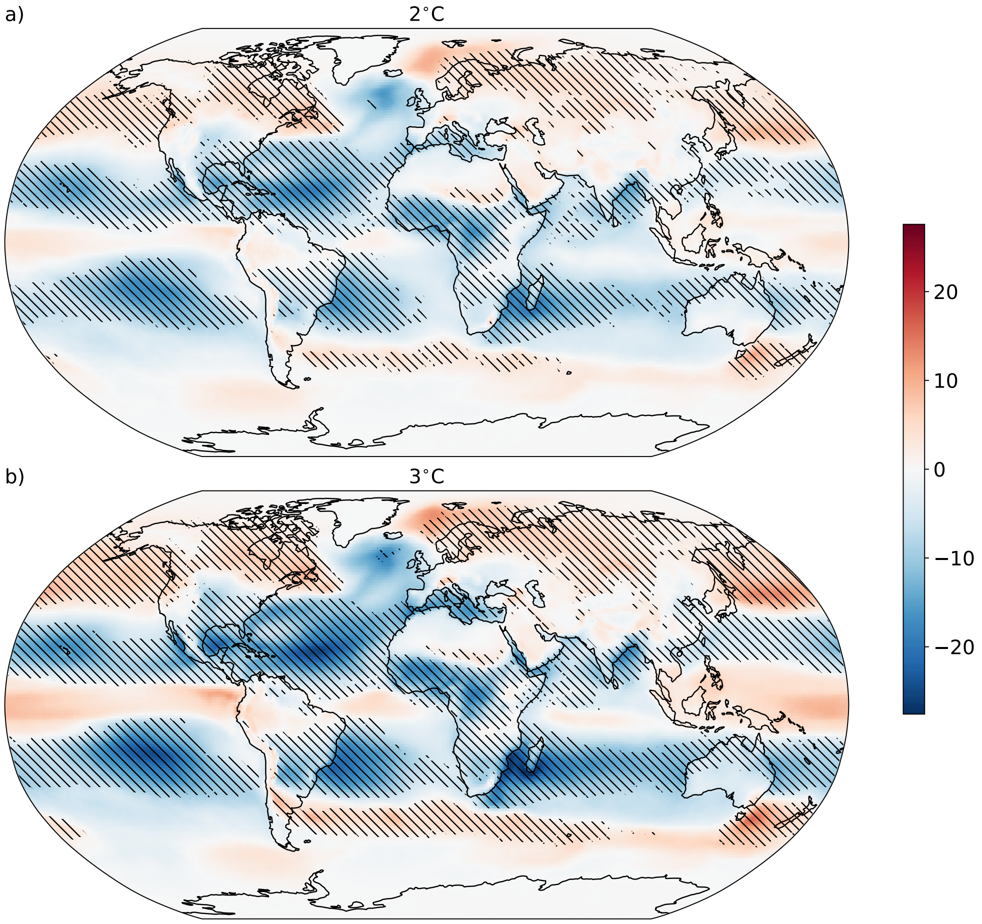

Fig. 2 **Hail-prone conditions shift under warming projections.** Multi-proxy, multimodel mean changes in annual hail-prone days for 2 °C (a) and 3 °C (b) of global warming. Stippling shows regions in which at least 50% of the model/proxy combinations agreed with the sign of the mean difference and also showed significant differences in the mean ($p < 0.05$ on a t-test on two related samples).

Figure 5 shows the main drivers of projected changes in this study, shown as the difference between these projected changes and changes when the future values for single ingredients were artificially de-biased. The ingredients driving the changes depend on the proxy. Overall, increases in instability drive increases in hail-prone environment frequency while increases in temperature-related ingredients drive reductions in hail-prone environment occurrence. The sums of changes across de-biased ingredients are close to the projected changes where no ingredients were de-biased, indicating that this experiment explains most of the projected changes, with the small differences that remain likely related to interactions between ingredients. The large differences between the proxy of [28] and the other proxies are caused by Eccel's proxy reacting to increases in instability without taking temperature changes into account. Changes

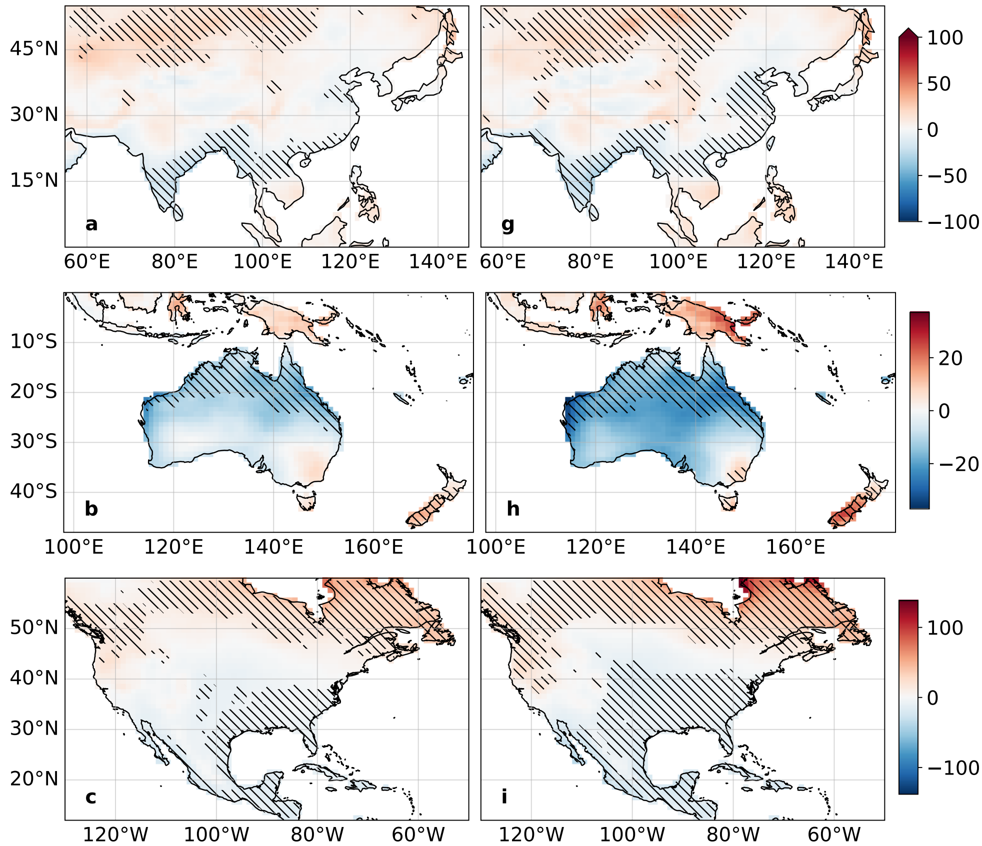

Fig. 3 Multi-proxy, multimodel mean changes in annual hail-prone days by region. Changes are shown as a percentage of multi-proxy, multimodel mean historical hail-prone days over land, for 2 °C warming (a-c) and 3 °C warming (g-i) for Asia (a, g), Australasia (b, h), and North America (c, i). Stippling as for Figure 2. Colour bars are shared across rows; to increase contrast the colour bar for a and g is truncated.

in SHIP are driven mainly by changes in the most-unstable mixing ratio. In the Raupach proxies, increases owing to instability increases are offset by changes in melting level height and T_{500}.

Changes in hail-prone days in cropping periods

For the historic period, the most hail-prone crops are millet, sorghum, soybeans, maize, groundnuts/peanuts, pulses, and wheat in the African tropics (Supplementary Figure 10). Warming of 2 °C and 3 °C is projected to reduce the hail-prone cropping period for these crops while increasing the risk for crops grown in more poleward regions (Supplementary Figures 11 and 12).

Figure 6 shows changes in the proportion of crop growing time that is considered hail-prone, by world region (regional maps of relative projected changes per crop are shown in Supplementary Figures 13, 14, 15, 16, 17 and 18). In Africa, all crops are

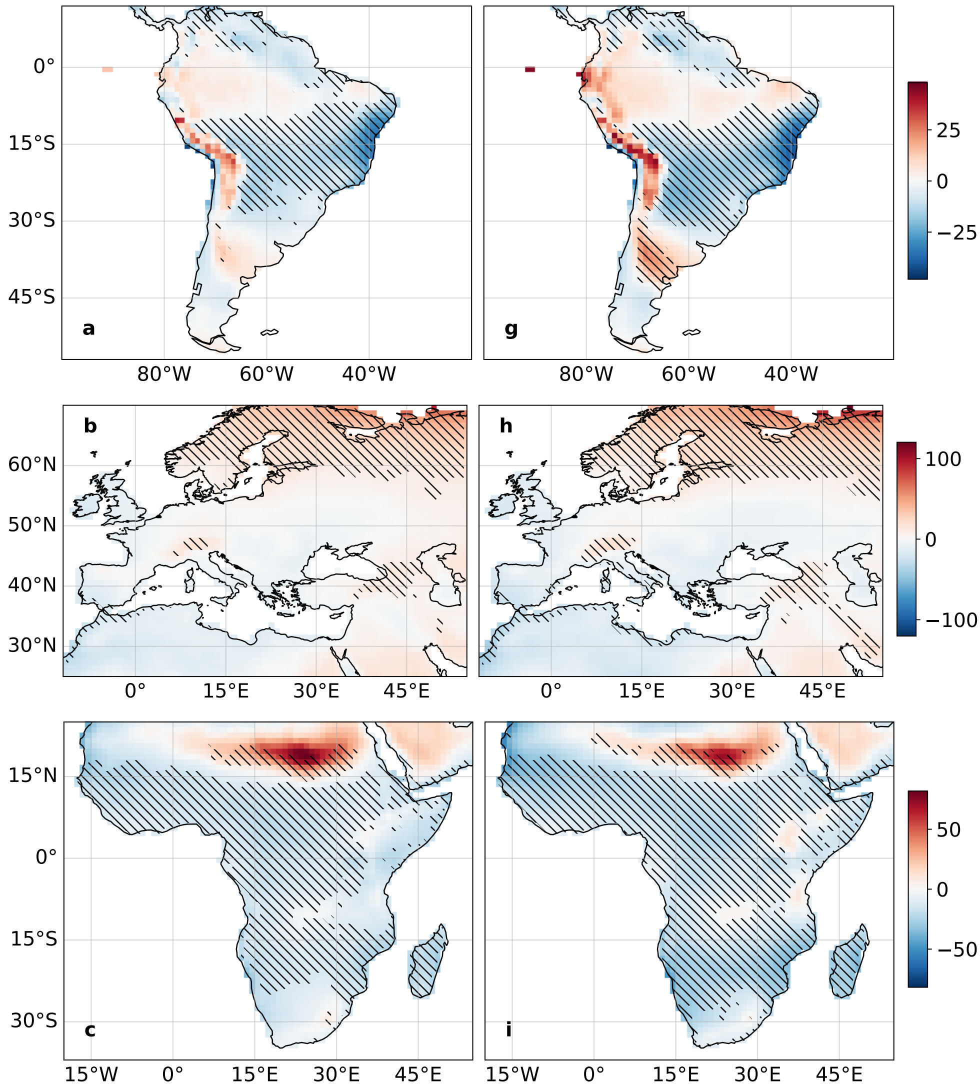

Fig. 4 As for Figure 3 but for South America (a, g), Europe (b, h), and Africa (f, i).

projected to experience fewer hail-prone days. Likewise in South America, all crops show projected decreased risk, with possible increases for barley, millet, and rye in the 3 °C scenario. In Asia and Europe, the crops of barley, fodder grasses, grapes/vine, rye, and wheat show particular projected increases in risk in the future scenarios. In Oceania, barley shows a projected increase in risk while all other crops show projected decreases in risk. Examinations of monthly changes for point locations (Supplementary Figures 19 and 20) highlight that the crops with the greatest increases in risk are those with winter cropping periods, while those with the greatest reductions in risk are those that grow across summer periods. **(More regional analysis.)**

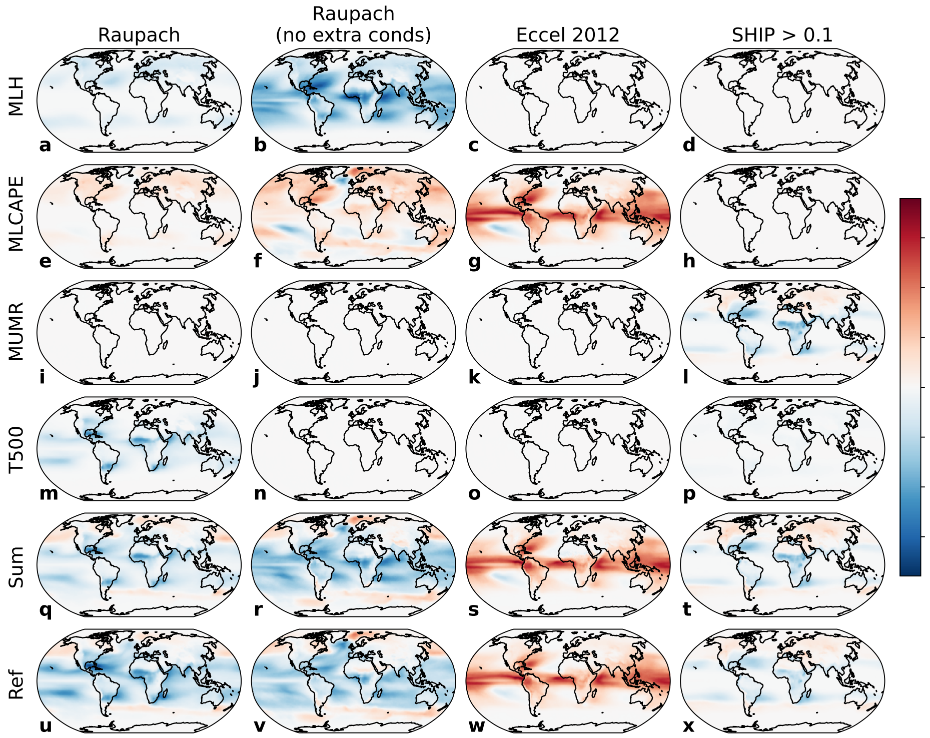

Fig. 5 The main drivers of the projected changes (all drivers are shown in Supplementary Figure 21). All plots are multimodel means. Plots show the difference in hail prone days between historical and the 3C epoch for unchanged ingredients, minus the difference with the given ingredient de-biased in the 3C epoch. Red (blue) areas show where an ingredient added to (subtracted from) the projected change. Ingredients shown here are melting level height (MLH, a-d), mixed-layer CAPE (MLCAPE, e-h), most-unstable mixing ratio (MUMR, i-l), and temperature at 500 hPa (T500, m-p). "Sum" (q-t) shows sums across changes from all de-biased ingredients (that is, column sums from Supplementary Figure 21) and "Ref" (u-x) shows the projected changes per proxy when no ingredients were de-biased. Columns show hail proxies and the colour scale is in annual hail days.

Discussion

- Although we show proxy results globally, the proxies used were trained using land-based reports [14, 28] and there is uncertainty in the occurrence of hail in maritime storms [8].
- Leung et al., 2023 also observed a northward shift in hailstorms in the US from 2000 (preprint at https://assets.researchsquare.com/files/rs-3217821/v1_covered_a256d1b8-b2e0-41b6-ab9c-e2628059bc91.pdf?c=1699615569.)
- It is clear that Eccel 2012 shows an increase where the Raupach proxies and SHIP show decreases. This is explained by the non-Eccel proxies taking changes in temperature explicitly into account, but the discrepancy also increases the uncertainty in these results.

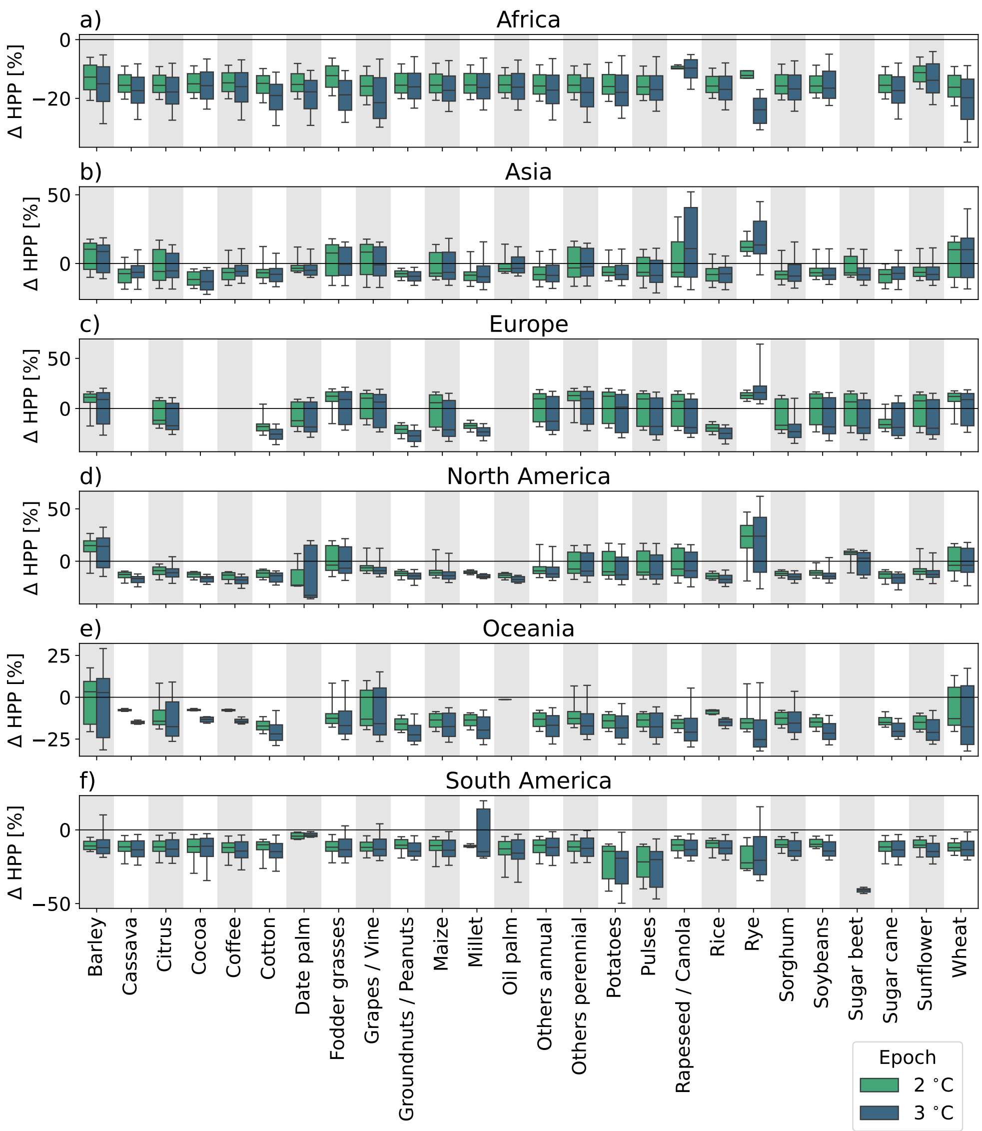

Fig. 6 Distributions of significant changes in hail-prone crop proportion (HPP) by crop, epoch, and world region. Regions are defined as in Figure 3. Changes multimodel, multi-proxy mean changes shown as a percentage of the multimodel, multi-proxy mean historical hail-prone crop proportion. Significant changes are those for which at least 50% of the model/proxy combinations agreed with the sign of the mean difference and also showed significant differences in the mean ($p < 0.05$ using Welch's t-test). Coloured boxes show interquartile ranges, whiskers show 10th-90th percentile ranges.

Online methods

Data

A filtering approach was used to select models from the Coupled Model Intercomparison Project Phase 6 (CMIP6) [7]. We selected models that contained variables required to calculate convective indices: air temperature at the surface (`tas`) and by model level (`ta`), wind vectors at the surface (`uas` and `vas`) and by level (`ua` and `va`), specific humidity at the surface (`huss`) and by level (`hus`), and surface pressure (`ps`). We filtered for models with a temporal resolution higher than six-hourly (those with "table IDs" of `3hr` or `6hrLev`), and models that were available for both historical and SSP5-8.5 experiments ("experiment IDs" of `historical` or `ssp585`). Further, the models had to be available in the National Computational Infrastructure (NCI) node of the Earth System Grid Federation (ESGF), and had to cover the required epochs. The resulting CMIP6 models, that we used here, are detailed in Supplementary Table 1. If model orography was available in the `orog` variable, it was used; if not, the orography of the historical runs of CNRM-CM6-1 (ensemble r1i1p1f2) was interpolated onto the model grid and used instead [29]. Reanalyses were European Centre for Medium-range Weather Forecasts (ECMWF) reanalysis 5 (ERA5) data [30] on pressure levels [31]. To match the CMIP6 model characteristics, we used global ERA5 data at 00, 06, 12, and 18 UTC for each day from 1980 to 1999, interpolated to 1×1 ° resolution.

Calculation of convective parameters

Convective parameters were calculated as described for the proxy of Raupach et al., 2023 [14], for each CMIP6 dataset at its native resolution and to ERA5 at the downscaled resolution. For each CMIP6 model, annual and seasonal statistics were calculated, then all statistics were interpolated onto a 1×1 ° spatial grid for comparison.

Application of hail proxies

We applied four hail-specific instability-shear proxies to CMIP6 and ERA5 data. The proxies were those modified versions of Raupach et al., 2023 (with and without "extra conditions" to remove false positives) [14], Eccel et al., 2012 [28], and a threshold of 0.1 on the Significant Hail Parameter (SHIP) [23]. The modifications made to the proxies of [14] are detailed in Supplementary Material Section 1. The proxies of Kunz 2007 [32] and Mohr and Kunz, 2013 [33] were tested but were found to produce unrealistically many hail-prone days in tropical regions for which they were not trained [14] (Supplementary Figure 22). Similarly, the threshold of 0.5 on SHIP, as has been used in other studies for severe hail [6], was found to produce too few hail-prone days in comparison with the other proxy results which are for any hail (Supplementary Figure 22), and was therefore excluded here.

Per-degree framework

The historical period used for each model was 1980–1999. The epochs that represented 2 °C and 3 °C warming compared to the historical period were determined per model using 20-year running means of monthly global average temperature anomalies (Supplementary Figure 23).

Calculation of drivers

For each hail proxy ingredient, de-biased versions of the 3 °C epoch were calculated using `python-cmethods` v2.3.0 [34] using the quantile-mapping method with 100 quantiles and the historical period as the baseline.

Data availability. MIRCA2000 data are available with identifier https://doi.org/10.5281/zenodo.7422506.

Code availability. Convective indices were calculated using `xarray_parcel` by T. H. Raupach (https://doi.org/10.5281/zenodo.8088497) **(Update version with new xarray release)**. Warming levels were calculated using code by T. H. Raupach **(ref)**.

Acknowledgements. This research was undertaken with the assistance of resources and services from the NCI, which is supported by the Australian Government. THR acknowledges financial support from QBE Insurance.

Competing interests. Since March 2024 THR's position at UNSW Sydney has been financially supported by QBE Insurance. The authors declare no other competing financial or non-financial interests.

Author contributions.

References

[1] Allen, J. T. *Climate Change and Severe Thunderstorms*, 67 (Oxford Univ. Press, 2018). URL https://oxfordre.com/climatescience/view/10.1093/acrefore/9780190228620.001.0001/acrefore-9780190228620-e-62.

[2] Brimelow, J. *Hail and Hailstorms* (Oxford Univ. Press, 2018). URL https://oxfordre.com/climatescience/view/10.1093/acrefore/9780190228620.001.0001/acrefore-9780190228620-e-666.

[3] Raupach, T. H. *et al.* The effects of climate change on hailstorms. *Nat. Rev. Earth Environ.* **2**, 213–226 (2021).

[4] Cecil, D. J. & Blankenship, C. B. Toward a global climatology of severe hailstorms as estimated by satellite passive microwave imagers. *J. Climate* **25**, 687–703 (2012).

[5] Bang, S. D. & Cecil, D. J. Constructing a multifrequency passive microwave hail retrieval and climatology in the GPM domain. *J. Appl. Meteorol.* **58**, 1889–1904 (2019).

[6] Prein, A. F. & Holland, G. J. Global estimates of damaging hail hazard. *Weather Clim. Extremes* **22**, 10–23 (2018).

[7] Eyring, V. *et al.* Overview of the Coupled Model Intercomparison Project Phase 6 (CMIP6) experimental design and organization. *Geosci. Model Dev.* **9**, 1937–1958 (2016).

[8] Knight, C. A. & Knight, N. C. in *Hailstorms* (ed.Doswell, C. A.) *Severe Convective Storms* 223–254 (American Meteorological Society, Boston, MA, 2001).

[9] Fraile, R., Castro, A., López, L., Sánchez, J. L. & Palencia, C. The influence of melting on hailstone size distribution. *Atmos. Res.* **67-68**, 203–213 (2003).

[10] Brooks, H. E., Lee, J. W. & Craven, J. P. The spatial distribution of severe thunderstorm and tornado environments from global reanalysis data. *Atmos. Res.* **67-68**, 73–94 (2003). European Conference on Severe Storms 2002.

[11] Brooks, H. E. Severe thunderstorms and climate change. *Atmos. Res.* **123**, 129–138 (2013).

[12] Dennis, E. J. & Kumjian, M. R. The impact of vertical wind shear on hail growth in simulated supercells. *J. Atmos. Sci.* **74**, 641–663 (2017).

[13] Lin, Y. & Kumjian, M. R. Influences of CAPE on hail production in simulated supercell storms. *J. Atmos. Sci.* **79**, 179–204 (2022).

[14] Raupach, T. H., Soderholm, J., Protat, A. & Sherwood, S. C. An improved instability–shear hail proxy for australia. *Mon. Weather Rev.* **151**, 545–567 (2023).

[15] Sherwood, S. C. Convective precursors and predictability in the tropical western Pacific. *Mon. Weather Rev.* **127**, 2977–2991 (1999).

[16] Tippett, M. K., Allen, J. T., Gensini, V. A. & Brooks, H. E. Climate and hazardous convective weather. *Curr. Clim. Change Rep.* **1**, 60–73 (2015).

[17] Seeley, J. T. & Romps, D. M. Why does tropical convective available potential energy (CAPE) increase with warming? *Geophys. Res. Lett.* **42**, 10,429–10,437 (2015).

[18] Prein, A. F. & Heymsfield, A. J. Increased melting level height impacts surface precipitation phase and intensity. *Nat. Clim. Change* **10**, 771–776 (2020).

[19] Mahoney, K., Alexander, M. A., Thompson, G., Barsugli, J. J. & Scott, J. D. Changes in hail and flood risk in high-resolution simulations over Colorado's mountains. *Nat. Clim. Change* **2**, 125–131 (2012).

[20] Diffenbaugh, N. S., Scherer, M. & Trapp, R. J. Robust increases in severe thunderstorm environments in response to greenhouse forcing. *P. Natl. Acad. Sci. USA* **110**, 16361–16366 (2013).

[21] Rädler, A. T., Groenemeijer, P. H., Faust, E., Sausen, R. & Púčik, T. Frequency of severe thunderstorms across Europe expected to increase in the 21st century due to rising instability. *npj Clim. Atmos. Sci.* **2**, 30 (2019).

[22] Lepore, C., Abernathey, R., Henderson, N., Allen, J. T. & Tippett, M. K. Future global convective environments in CMIP6 models. *Earth's Future* **9**, e2021EF002277 (2021).

[23] NOAA SPC. Significant hail parameter. https://www.spc.noaa.gov/exper/mesoanalysis/help/help_sigh.html (2022). National Oceanographic and Atmospheric Administration National Weather Service Storm Prediction Center, accessed 21 June 2022.

[24] Singh, S. K., Saxena, R., Porwal, A., Ray, N. & Ray, S. S. Assessment of hailstorm damage in wheat crop using remote sensing. *Curr Sci India* **112**, 2095–2100 (2017).

[25] Pucik, T. Major hailstorms of 2022 (2023). URL https://www.essl.org/cms/major-hailstorms-of-2022/. Accessed 2024-01-10.

[26] Soyka, T. Severe 2022 hail damage in france sets new benchmarks, underscores shift of risk and calls for pricing adjustments (2023). URL https://www.swissre.com/risk-knowledge/mitigating-climate-risk/hail-damage-risk-france-2022.html. Accessed 2024-01-10.

[27] Chattopadhyay, N., Devi, S. S., John, G. & Choudhari, V. Occurrence of hail storms and strategies to minimize its effect on crops. *Mausam* **68**, 75–92 (2017).

[28] Eccel, E., Cau, P., Riemann-Campe, K. & Biasioli, F. Quantitative hail monitoring in an alpine area: 35-year climatology and links with atmospheric variables. *Int. J. Climatol.* **3**, 503–517 (2012).

[29] Bracegirdle, T. J. *et al.* Twenty first century changes in Antarctic and Southern Ocean surface climate in CMIP6. *Atmos. Sci. Lett.* **21**, e984 (2020).

[30] Hersbach, H. *et al.* The ERA5 global reanalysis. *Q. J. Roy. Meteor. Soc.* **146**, 1999–2049 (2020).

[31] Hersbach, H. *et al.* ERA5 hourly data on pressure levels from 1979 to present (2018). Copernicus Climate Change Service (C3S) Climate Data Store (CDS).

[32] Kunz, M. The skill of convective parameters and indices to predict isolated and severe thunderstorms. *Nat. Hazards Earth Sys.* **7**, 327–342 (2007).

[33] Mohr, S. & Kunz, M. Recent trends and variabilities of convective parameters relevant for hail events in Germany and Europe. *Atmos. Res.* **123**, 211–228 (2013).

[34] Schwertfeger, B. T. btschwertfeger/python-cmethods: v2.3.0 (2024). URL https://doi.org/10.5281/zenodo.12168002.